AFRL-AFOSR-JP-TR-2023-0076

Sustainable Soda Lignin-PLA 3D Printable Biocomposite Materials

Suhr, Jonghwan
Sungkyunkwan University Research & Business
2066 Seobu-ro, Jangan-gu
Suwon,, , 16419
KR

04/04/2023
Final Technical Report

Air Force Research Laboratory
Air Force Office of Scientific Research
Asian Office of Aerospace Research and Development
Unit 45002, APO AP 96338-5002

REPORT DOCUMENTATION PAGE

PLEASE DO NOT RETURN YOUR FORM TO THE ABOVE ORGANIZATION.

1. REPORT DATE	2. REPORT TYPE	3. DATES COVERED	
20230404	Final	START DATE 20190927	END DATE 20210926

4. TITLE AND SUBTITLE
Sustainable Soda Lignin-PLA 3D Printable Biocomposite Materials

5a. CONTRACT NUMBER	5b. GRANT NUMBER	5c. PROGRAM ELEMENT NUMBER
FA2386-19-1-4082		
5d. PROJECT NUMBER	**5e. TASK NUMBER**	**5f. WORK UNIT NUMBER**

6. AUTHOR(S)
Jonghwan Suhr

7. PERFORMING ORGANIZATION NAME(S) AND ADDRESS(ES)
Sungkyunkwan University Research & Business
2066 Seobu-ro, Jangan-gu
Suwon, 16419
KR

8. PERFORMING ORGANIZATION REPORT NUMBER

9. SPONSORING/MONITORING AGENCY NAME(S) AND ADDRESS(ES)	10. SPONSOR/MONITOR'S ACRONYM(S)	11. SPONSOR/MONITOR'S REPORT NUMBER(S)
AOARD UNIT 45002 APO AP 96338-5002	AFRL/AFOSR IOA	AFRL-AFOSR-JP-TR-2023-0076

12. DISTRIBUTION/AVAILABILITY STATEMENT
A Distribution Unlimited: PB Public Release

13. SUPPLEMENTARY NOTES

14. ABSTRACT
The development and manufacturing of lignin--based composites have shown promising results based composites have shown promising results towards the sustainable development of green materials. However, the high brittleness and poor towards the sustainable development of green materials. However, the high brittleness and poor processability of composites restrict their potential applications, cauprocessability of composites restrict their potential applications, caused by the lignin's weak sed by the lignin's weak compatibility with conventional polymers and its high viscosity. In this study, compatibility with conventional polymers and its high viscosity. In this study, soda lignin was soda lignin was extracted from oil palm empty fruit bunches (OPEFB), and extracted from oil palm empty fruit bunches (OPEFB), and a higha high--performance, printable performance, printable ligninlignin--based polylactic acid (PLA) composite wasbased polylactic acid (PLA) composite was devised through copolymerizing 2devised through copolymerizing 2--Ethylhexyl acrylate at the interface. It was shown that 10 wt% modified lignin (eEthylhexyl acrylate at the interface. It was shown that 10 wt% modified lignin (e--lignin) lignin) composites exhibit enhanced toughness from 1.16 to 3.84 MJ/mcomposites exhibit enhanced toughness from 1.16 to 3.84 MJ/m33 and impact energy from 2.12 and impact energy from 2.12 to 6.36 KJ/mto 6.36 KJ/m22 relative to the pure PLA, whrelative to the pure PLA, while also showile also showinging appropriate melt viscosity during appropriate melt viscosity during fused deposition modeling. Additionally, the low melt viscosity of the dispersed efused deposition modeling. Additionally, the low melt viscosity of the dispersed e--Lignin phase Lignin phase induces local thermoinduces local thermo--rheological relaxation facilitating the mobility of PLA molecular chains. rheological relaxation facilitating the mobility of PLA molecular chains. Notable that aNotable that adhesion between deposited layers was increased due to high interfacial diffusion dhesion between deposited layers was increased due to high interfacial diffusion of composites, where more than twice weld energy was achieved in 10 wt% eof composites, where more than twice weld energy was achieved in 10 wt% e--lignin filaments lignin filaments compared to those of pure PLA. Finally, the toughening mechanism was interpreted by compared to those of pure PLA. Finally, the toughening mechanism was interpreted by the the plasticization and the bridging effect of eplasticization and the bridging effect of e--Lignin. This study presents a method of utilizing Lignin. This study presents a method of utilizing lignin to replace petroleumlignin to replace petroleum--based thermoplastics, generally used in additive manufacturing based thermoplastics, generally used in additive manufacturing with exceptional mechanical performance.with exceptional mechanical performance.

15. SUBJECT TERMS

16. SECURITY CLASSIFICATION OF:			17. LIMITATION OF ABSTRACT	18. NUMBER OF PAGES
a. REPORT	b. ABSTRACT	c. THIS PAGE		
U	U	U	SAR	24

19a. NAME OF RESPONSIBLE PERSON	19b. PHONE NUMBER *(Include area code)*
JEREMY KNOPP	315-227-7006

Standard Form 298 (Rev.5/2020)
Prescribed by ANSI Std. Z39.18

AFRL-AFOSR-2019-4082

SUSTAINABLE SODA LIGNIN-PLA 3D PRINTABLE BIOCOMPOSITE MATERIALS

Jonghwan Suhr

Sungkyunkwan University

09/2021

Final Report

NOTICE AND SIGNATURE PAGE

Using Government drawings, specifications, or other data included in this document for any purpose other than Government procurement does not in any way obligate the U.S. Government. The fact that the Government formulated or supplied the drawings, specifications, or other data does not license the holder or any other person or corporation; or convey any rights or permission to manufacture, use, or sell any patented invention that may relate to them.

This report is the result of contracted fundamental research deemed exempt from public affairs security and policy review in accordance with SAF/AQR memorandum dated 10 Dec 08 and AFRL/CA policy clarification memorandum dated 16 Jan 09. This report is available to the general public, including foreign nationals. Copies may be obtained from the Defense Technical Information Center (DTIC) (http://www.dtic.mil).

FA2386-19-1-4082 HAS BEEN REVIEWED AND IS APPROVED FOR PUBLICATION.

REPORT DOCUMENTATION PAGE

Form Approved
OMB No. 0704-0188

1. REPORT DATE *(DD-MM-YYYY)*	**2. REPORT TYPE**	**3. DATES COVERED** *(From - To)*
16/12/2021	FINAL	27/09/2019 – 26/09/2021

4. TITLE AND SUBTITLE

Sustainable Soda Lignin-PLA 3D Printable Biocomposite Materials

5a. CONTRACT NUMBER

5b. GRANT NUMBER
FA2386-19-1-4082

5c. PROGRAM ELEMENT NUMBER

6. AUTHOR(S)

Jonghwan Suhr

5d. PROJECT NUMBER

5e. TASK NUMBER

5f. WORK UNIT NUMBER

7. PERFORMING ORGANIZATION NAME(S) AND ADDRESS(ES)

Sunkyunkwan University
2066, Seobu-ro, Jangan-gu,
Suwon-si, Gyeonggi-do,
Republic of Korea 16419

8. PERFORMING ORGANIZATION REPORT

9. SPONSORING / MONITORING AGENCY NAME(S) AND ADDRESS(ES)

Air Force Research
Airman Systems Directorate
Wright-Patterson Air Force
45433

10. SPONSOR/MONITOR'S ACRONYM(S)

AFRL/RHC

11. SPONSOR/MONITOR'S REPORT NUMBER(S)

AFRL-RH-WP-TR-2019-4082

12. DISTRIBUTION / AVAILABILITY STATEMENT

DISTRIBUTION STATEMENT A: Approved for public release; distribution unlimited.

13. SUPPLEMENTARY NOTES

Lignin-g-2-Ethylhexyl acrylate; PLA; 3D printability; mechanical properties; toughening mechanism

14. ABSTRACT

The development and manufacturing of lignin-based composites have shown promising results towards the sustainable development of green materials. However, the high brittleness and poor processability of composites restrict their potential applications, caused by the lignin's weak compatibility with conventional polymers and its high viscosity. In this study, soda lignin was extracted from oil palm empty fruit bunches (OPEFB), and a high-performance, printable lignin-based polylactic acid (PLA) composite was devised through copolymerizing 2-Ethylhexyl acrylate at the interface. It was shown that 10 wt% modified lignin (e-lignin) composites exhibit enhanced toughness from 1.16 to 3.84 MJ/m^3 and impact energy from 2.12 to 6.36 KJ/m^2 relative to the pure PLA, while also showing appropriate melt viscosity during fused deposition modeling. This study presents a method of utilizing lignin to replace petroleum-based thermoplastics, generally used in additive manufacturing with exceptional mechanical performance.

15. SUBJECT TERMS

16. SECURITY CLASSIFICATION OF:			**17. LIMITATION OF ABSTRACT**	**18. NUMBER OF PAGES**	**19a. NAME OF RESPONSIBLE PERSON**
					AFRLWUM
a. REPORT	**b. ABSTRACT**	**c. THIS PAGE**			**19b. TELEPHONE NUMBER** *(include area code)*
Unclassified	Unclassified	Unclassified	SAR	18	

Standard Form 298 (Rev. 8-98)
Prescribed by ANSI Std. Z39.18

TABLE OF CONTENTS

Section Page

LIST OF FIGURES

Page

LIST OF TABLES

Page

1.0 SUMMARY

The development and manufacturing of lignin-based composites have shown promising results towards the sustainable development of green materials. However, the high brittleness and poor processability of composites restrict their potential applications, caused by the lignin's weak compatibility with conventional polymers and its high viscosity. In this study, soda lignin was extracted from oil palm empty fruit bunches (OPEFB), and a high-performance, printable lignin-based polylactic acid (PLA) composite was devised through copolymerizing 2-Ethylhexyl acrylate at the interface. It was shown that 10 wt% modified lignin (e-lignin) composites exhibit enhanced toughness from 1.16 to 3.84 MJ/m^3 and impact energy from 2.12 to 6.36 KJ/m^2 relative to the pure PLA, while also showing appropriate melt viscosity during fused deposition modeling. Additionally, the low melt viscosity of the dispersed e-Lignin phase induces local thermo-rheological relaxation facilitating the mobility of PLA molecular chains. Notable that adhesion between deposited layers was increased due to high interfacial diffusion of composites, where more than twice weld energy was achieved in 10 wt% e-lignin filaments compared to those of pure PLA. Finally, the toughening mechanism was interpreted by the plasticization and the bridging effect of e-Lignin. This study presents a method of utilizing lignin to replace petroleum-based thermoplastics, generally used in additive manufacturing with exceptional mechanical performance.

2.0 INTRODUCTION

Recently, the importance of polymers has been much more emphasized because of their wide applications in different fields of science, technology, and industry. Among various polymers, petroleum-based synthetic polymers are the most prevalent commodity on earth. However, the long-term effects of using these materials, including the consumption of petroleum raw materials, the high cost of related manufacturing technologies, and the non-degradable waste generated, are threatening to the environment [1-3]. Therefore, efforts have been made to use eco-friendly materials and technologies to improve environmental sustainability.

For several decades, the development of biomass materials along with their additive manufacturing processes has received increasing attention. Cellulose [4], lignin [5, 6], starch [7], and other biomass-derived substances [8] have been utilized in fused deposition modeling, stereolithography, binder jetting, or direct ink writing 3D printing technologies [9-12]. The use of these biomass substances for analytical, dental, medical, orthopedic, consumer testing, and food applications can be extremely beneficial owing to their low cost, recyclability, biodegradability, and relatively low density [13, 14].

Lignin is an ideal candidate for the development of biomass sustainable composites due to its high abundance, extremely low cost, biodegradability, and other special properties, (i.e., antioxidant, antimicrobial, and UV blocking). Gkartzou et al. first researched polylactic acid (PLA)/lignin composites for 3D printing and optimized the parameters in the printing process [15]. They found that increasing lignin content resulted in severe material brittleness and high

melting apparent viscosity during extrusion, showing the maximum amount of lignin was 15 wt% with around 60% decrease of elongation relative to pure PLA. Subsequently, various plasticizers or elastic materials are blended to reduce the melt viscosity of the composite to accommodate more lignin. Wasti et al. added two plasticizers (polyethylene glycol (PEG) 2000 and struktol TR451) in varying concentrations to obtain PLA/lignin composite filaments, and PLA was replaced with lignin up to 20 wt% [16]. Additionally, a 40 wt% lignin-based acrylonitrile butadiene styrene (ABS) composites containing acrylonitrile-butadiene rubber (NBR41, 41 mol% nitrile content) and carbon fibers (CFs) were made by fused deposition modeling (FDM), wherein the composites exhibited good 3D printability and interlayer adhesion (Nguyen et al., 2018) [17]. However, in these studies, increasing the amount of added lignin is considered an effective way to enhance the biodegradability of the matrix [18], while the mechanical properties of resultant composites were ignored. The incorporation of lignin into the matrix often leads to a decrease in tensile strength and elongation [19, 20], which is caused by poor compatibility at the interface between the filler and matrix due to the hydrophilicity of biomass material and the hydrophobicity of most polymer resins [21]. The lack of interfacial interaction not only causes poor dispersion and significantly reduced mechanical properties, but also affects the melt rheology and processability of 3D printing [22]. Few studies have taken into account both the mechanical properties of materials and the processability of 3D printing through interface engineering.

Therefore, in this work, the interface of PLA/lignin composite was designed by chemical grafting to improve mechanical properties and 3D printability. First, lignin was modified by copolymerizing 2-Ethylhexyl acrylate (EHA) to improve its interfacial compatibility with PLA, then the rheology, mechanical properties, and interlay adhesion of the composites in 3D printing were investigated. Modified lignin (e-Lignin) exhibits homogeneous dispersion and good interfacial compatibility with PLA. In terms of the mechanical properties, 10 wt% e-Lignin/PLA composite showed the highest toughness (3.84 MJ/m^3) and impact energy (6.36 KJ/m^2), respectively, was designed with excellent 3D-printability and interlayer adhesion. Additionally, the plasticization mechanism and the bridging mechanism cooperatively explain the toughening mechanism in the composite. This study could show the great potential of using ductile PLA/e-Lignin biocomposite as a part to resist impact load and withstand vibration, designing through 3D printing.

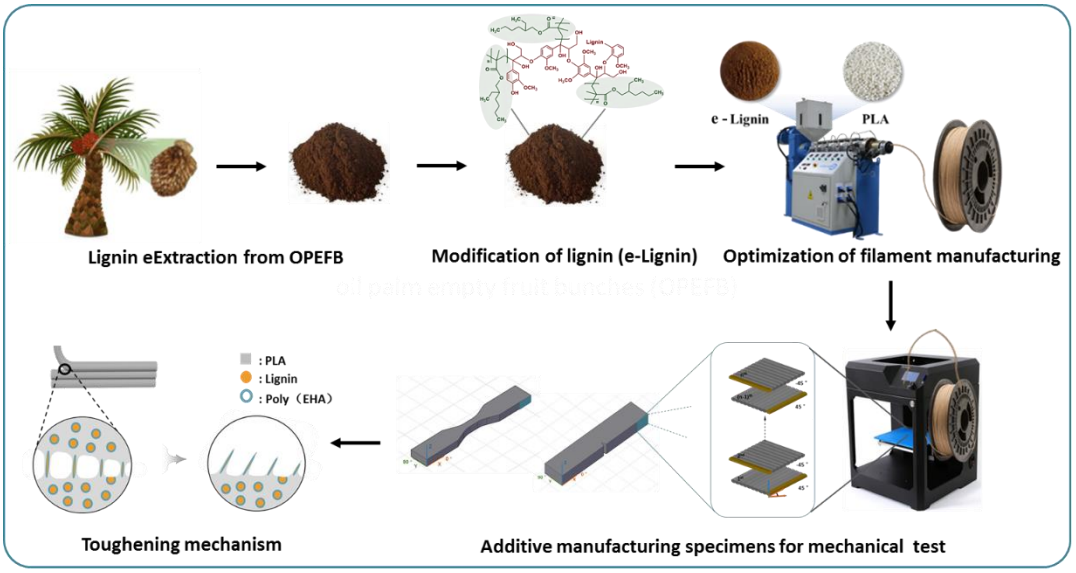

Fig. 1. Schematic of the full text.

3.0 METHODS, ASSUMPTIONS, AND PROCEDURES

3.1 Materials

Oil palm empty fruit bunches (OPEFB) were obtained from the local palm oil mill. PLA pellets (Luminy LX175, density 1.24 g/cm^3) were purchased from Total Corbion PLA company, Holland. Kraft lignin was obtained from Moorim Pulp & Paper Co., South Korea. Sodium chloride (NaCl), dimethyl sulfoxide (DMSO), 2-Ethylhexyl acrylate (EHA), hydrogen peroxide (H_2O_2), hydrochloric acid (HCl), sodium hydroxide (NaOH), phosphoric acid (H_3PO4), ethanol, and methanol (CH_3OH) were purchased from Sigma-Aldrich.

3.2 Soda lignin extraction from oil palm empty fruit bunches (OPEFB)

Before the alkaline extraction process, the OPEFB was washed, dried, crushed, and sieved. Then the isolation of lignin has been done using the alkaline extraction method as explained below: The mixture of OPEFB fiber and NaOH solution was made to produce a solid/liquid ratio of 1:15 (w/v) in a 500 mL beaker at 90 ºC for 3h. The black liquor obtained was filtrated to separate the undissolved fibers and concentrated in the oven at 60 º C for 24h. Then, the concentrated black liquor was acidified to pH 2 using 20% H_3PO_4. After 24h, the precipitated lignin was filtered and washed with ethanol to remove impurities before being dried in the oven at 60 º C for 24h. The lignin cake obtained was dried in the oven at 55 º C for 24h. before grinding to produce lignin in powder.

3.3 Surface modification of soda lignin

10.5 g of NaCl was dissolved in 200 mL of DMSO under magnetic stirring and heating at 50 °C. Then 10 g of lignin was added to the mixture and stirred for 20 min to dissolve. Subsequently, 15 g of EHA and 10 mL of H_2O_2 were added to the solution. After 24 h, the graft

reaction was terminated by slowly pouring the solution into an excessively diluted HCl solution. Finally, the e-Lignin was obtained by filtration, washing with methanol, and drying in a vacuum oven at 60 °C for 24 h.

3.4 PLA/lignin blending and filament processing

The lignin or e-Lignin with different content were mixed with PLA pellets in the Haake rheometer (Thermo Haake Polydrive Mixer). The blends were then fed into a single screw extruder (Wellzoom E) to fabricate filaments under 180 °C. Subsequently, the blend pellets were prepared by cutting filaments through a pelletizer.

The blend pellets were poured into the single screw extruder, and the temperature of the extruder heating chamber and outlet nozzle was adjusted at 185 °C and 175 °C respectively. At the same time, the screw rotation speed and pulling speed were kept at 35 rpm and 0.9 m/min. Air cooling and water cooling were introduced between the extruder head to the spooler to enhance the filament cooling process. The blend filaments with a diameter of 1.75±0.2 mm were obtained by adjusting all these extrusion process parameters.

3.5 Preparation of 3D printed specimens for tensile, Izod impact, and tear test

Two sets of tensile specimens were prepared through conventional injection molding and 3D printing according to the standard ASTM D638 type V. The dimensions of 3D printed tensile and impact specimens were shown in Fig. 2. To fabricate specimens for the Izod impact test, samples were printed without a notch firstly, then the cutting wheel produced a notch with the specified size. All the FDM process parameters are summarized in Table 1.

Tear test specimens resembling walls one road thick and 16 roads tall were printed in the same direction as shown in Fig. S1c, and 100 mm long walls were printed to provide sufficient adhesion between different roads. After printing, a 16 mm pre-crack was introduced, then two parts were manually separated (Fig. 2c) and clamped in the opposing grips of the tensile Instron [23].

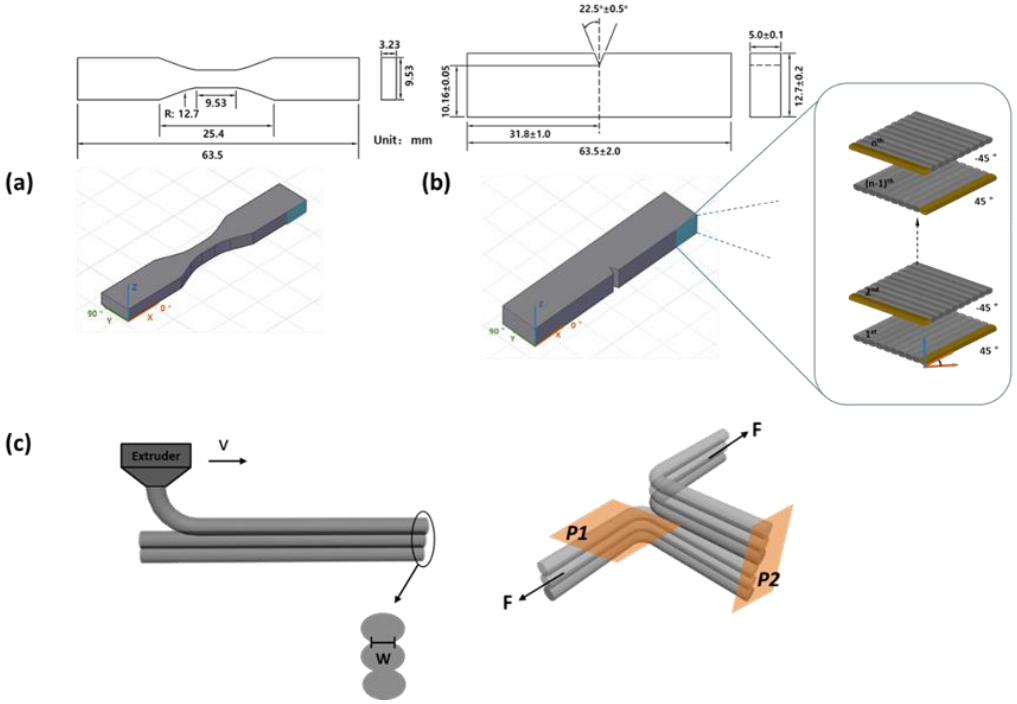

Fig. 2. Specimens standard for (a) tensile, (b) Izod impact, and (c) tear test.

Table 1. Fused deposition modeling parameters Printer: Cubicon 3 DP-210F

Variables	Values	Unit
Nozzle	Circular (0.4 mm dia.)	
Print orientation	45 °/-45 °	
Nozzle temperature	210	°C
Bed temperature	65	°C
Layer thickness	0.2	mm
Print velocity	40	mm/s
Infill density	100	%
Infill pattern	Linear	

3.6 Characterization

The grafting effect of lignin was qualitatively analyzed by FT-IR spectroscopy (Vertex 70, Bruker), ^{1}H nuclear magnetic resonance (NMR), and ^{13}C NMR (500 MHz, Bruker), where d-chloroform was used as the solvent. GPC (Agilent 1100 S) determined the weight average molecular weights (M_w) and number average molecular weights (M_n) quantitatively, using tetrahydrofuran as the solvent and mobile phases.

The surface tensions of lignin and e-Lignin were determined to evaluate their interfacial tension with the PLA. The dispersive (γ_s^d) and polar (γ_s^p) components of the surface tension (γ) were calculated using the Owens–Wendt equation given by,

$$\gamma_l(1+cos\theta) = 2\sqrt{\gamma_s^d \gamma_l^d} + 2\sqrt{\gamma_s^p \gamma_l^p}, \quad (1)$$

where θ is the contact angle measured by a contact angle meter (PHX 300, SEO), and γ_l, γ_l^d, and γ_l^p are the surface tension, dispersive component, and polar component of the test liquids, respectively. Deionized water (γ_l^d = 21.8 mJ/m^2, γ_l = 72.8 mJ/m^2) and diiodomethane (γ_l^d= 50.8 mJ/m^2, γ_l= 50.8 mJ/m^2, 99% purity, Alfa Aesar, USA) were used as test liquids. The interfacial tension between the lignin and PLA (A and B) was determined using Equation 2 [24].

$$\gamma_{AB} = \gamma_A + \gamma_B - 2\sqrt{\gamma_A^d \gamma_B^d} - 2\sqrt{\gamma_A^p \gamma_B^p} \quad (2)$$

The thermal properties of the composites were determined by differential scanning calorimetry (DSC) (Q200, TA Instruments) at a heating rate of 10 °C/min from −50 to 200 °C, and thermogravimetric analysis (TGA) (Q50, TA Instruments) in the temperature range of 25 to 800 °C at 20 ºC/min. The dynamic mechanical properties of the composites were measured using dynamic mechanical analysis (DMA) (Q800, TA Instruments) in tensile mode at a constant strain of 0.05% and an oscillating frequency of 1 Hz. The temperature was swept from 20 to 120 °C at 3 °C/min (specimen dimensions were 60 mm × 40 mm × 0.5 mm). At least three samples were tested for each ratio.

Tensile testing was performed using an ElectroPuls E3000 (Instron) with a 3 kN load cell and a cross-head speed of 10 mm/s. Impact tests were conducted using an Izod impact tester (TO-700). Five samples were tested for each ratio. Rheological measurements were taken on a rheometer (ARES-G2, TA Instruments) to evaluate the 3D printability of the composite. Frequency sweeps were performed from 0.1 to 1000 rad/s at 190 °C and a strain amplitude of 0.1%.

A tear test was conducted using an ElectroPuls E3000 (Instron) with a 500 N load cell and a cross-head speed of 100 mm/min to analyze the toughening mechanism further. The interlayer failure of the tear test specimens and the specimen cross-section after the impact test was observed by SEM (JSM-7500F, JEOL)

4.0 RESULTS AND DISCUSSION

4.1 Characterizations of soda lignin

The SEM image (Fig. 3a) demonstrates that lignin owns irregular shapes and uneven size distribution from Several micrometers to ten micrometers with a molecular weight of 4133 g/mol in table 2. For the FTIR (Fig. 3b), the vibrational band at 1530–1480 cm^{-1} is mostly attributed to the stretching of the C=C bonds, part of the aromatic skeletal of lignin molecules. Furthermore, the C=O stretching conjugated to the aromatic ring bending mode is assigned to the band at 1660–1720 cm^{-1}. Finally, the bands at 1490 and 1510 cm^{-1} can be assigned to the vibration modes of the aromatic rings in lignin. In addition, hydroxyl and methyl groups can

be found at 3460 and 2901 cm^{-1} respectively. The glass transition temperature of the lignin is around 160 ^{o}C shown in Fig. 3c.

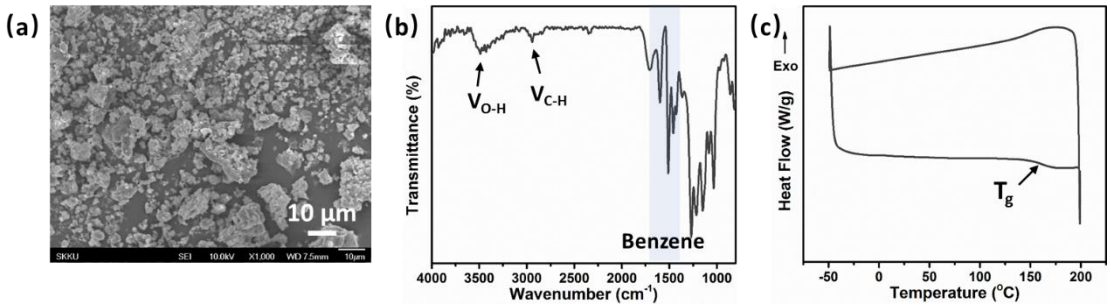

Fig. 3. (a) SEM, (b) FTIR, (c) DSC of lignin.

4.2 Characterizations of lignin grafting and interfacial effect

EHA was copolymerized onto lignin to achieve good interface compatibility between PLA and lignin. The FTIR spectra are employed to identify the functional group changes of the lignin before and after grafting shown in Fig. 4a. The lignin shows a broad peak at 3460 cm^{-1}, corresponding to the stretching vibration of the hydroxyl groups. In addition to the sharp peaks at 1604, 1509 and 1450 cm^{-1} represent aromatic skeletal vibrations. Besides, the peak at 1212 cm^{-1} is ascribed to phenolic C-O groups. After modification, two important peaks at 1731 cm^{-1} (-COO-) and 1163 cm^{-1} (C-O) indicate the acrylate group in the e-Lignin. Moreover, the absorption peaks between 3000 and 2840 cm^{-1} arise from the alkane chain of the EHA.

The ^{1}H NMR and ^{13}C NMR spectra are also conducted to further confirm the graft effect shown in Figs. 4b,c. The ^{1}H NMR spectrum shows the aromatic proton, methoxy proton, and methylene/ methine proton peaks of lignin at 6.0-8.0, 3.5-4.2, and 0.8-2.1 ppm respectively. After modification, the chemical shifts between 6.0 and 7.0 ppm for vinyl protons of the EHA monomer are not observed, confirming the polymerization onto the lignin through opening the C=C. Moreover, the methyl, methylene, and methine protons of the EHA chain including methylene protons near the ester bond show peaks in the range of 0.8-3.88 ppm. Additionally, the ^{13}C NMR spectrum of the e-Lignin shows chemical shifts at 11.6 and 14.1 ppm belonging to the carbon in the terminal methyl group of the EHA. The chemical shifts between 23.0-30.8 ppm are assigned to the carbon on the methylene group in the EHA long chain, whereas the carbon that is next to the ester group shows a peak at 67.8 ppm. The chemical shift at 39.6 ppm corresponds to the carbon atom in the methine group. The important carbon of the ester group shows a peak at 175.9 ppm due to the existence of EHA. Therefore, e-Lignin is successfully synthesized by copolymerizing the EHA onto lignin.

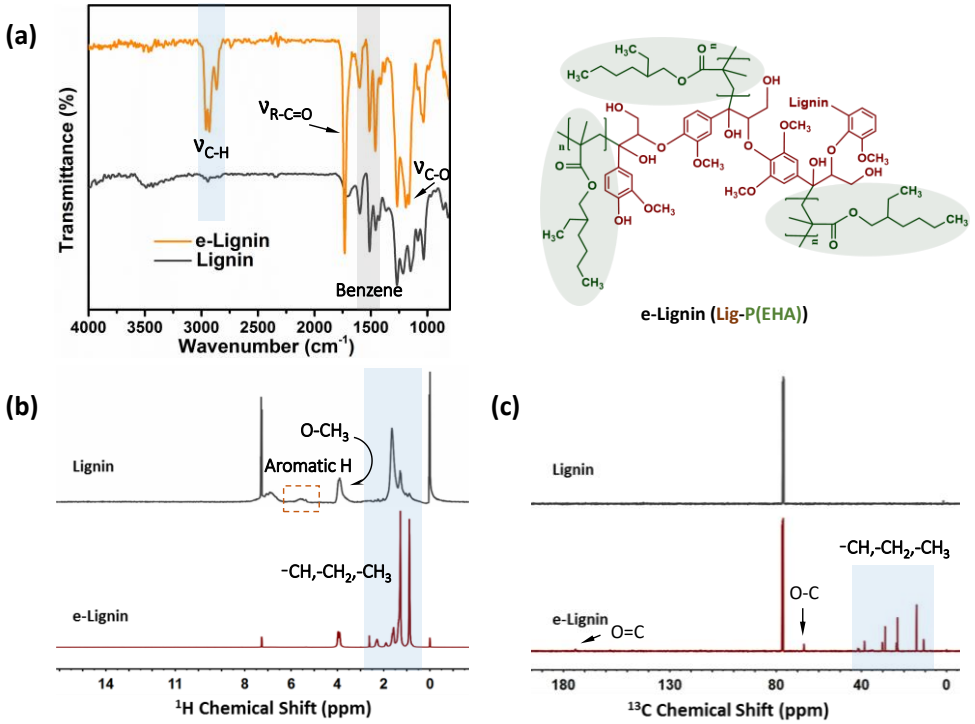

Fig. 4. (a) FTIR spectra, (b) ^{1}H NMR, and (c) ^{13}C NMR spectra of the lignin and e-Lignin.

GPC tests are performed to qualitatively determine the grafting effect. Table 2 shows the weight average molecular weight (Mw), number average molecular weight (Mn), and polydispersity index (PDI) of the lignin, e-Lignin, and PLA. The polymerization of EHA leads to an increased Mw and Mn (116 550 and 44 557 g/mol, respectively) with a higher PDI of 2.62, indicating a wider molecular weight distribution. Remarkable changes in the surface tension are also revealed from the contact angle results, which show that the hydrophilicity of the e-Lignin is reduced as the contact angle with water increases from 57.7° to 73.2°. This is because the hydrophobic poly (EHA) long-chain covers the lignin, reducing the relative content of the original hydroxyl groups. A large number of ester groups in the poly EHA also achieve a lower interfacial tension of 0.31 mN/m between e-Lignin (43.1 mN/m) and PLA (37.7 mN/m), indicating good compatibility of them.

Table 2. Molecular weight, surface tension, and interfacial tension of lignin, e-Lignin, and PLA

	Mw (g/mol)	Mn (g/mol)	PDI	Contact angle (°)		Surface tension (mN/m)			Interfacial tension with PLA (mN/m)
				Water	Diiodomethane	Dispersive component (γ^d)	Polar component (γ^p)	Total (γ)	
Lignin	4 133	2 141	1.93	57.7 ± 3.7	22.5 ± 2.6	47.0	11.0	58.0	2.63
e-Lignin	116 550	44 557	2.62	73.2 ± 2.3	46.1 ± 1.7	36.3	6.8	43.1	0.31
PLA	183 177	107 296	1.71	80.9 ± 1.1	51.9 ± 1.3	33.2	4.5	37.7	

4.3 Thermal and mechanical properties of PLA/Lignin composites

Fig. 5a shows the DSC curves of the PLA/e-Lignin composites during the second heating scan, presenting the T_g, the cold crystallization exotherm at T_{cc}, and the melting endotherm at T_m. Pure PLA shows a T_g of 62.24 °C while the exothermic peak is observed at 108.75 °C, and the endothermic melting peak is observed at 175.93 °C (Table 3). The addition of e-Lignin produces a shift to lower T_g, T_{cc}, and T_m of the PLA/e-Lignin composites. This effect could be explained by the low melt viscosity of the dispersed e-Lignin phase inducing local thermo-rheological relaxation, resulting in increasing molecular mobility of the polymer chain and leading to a greater degree of macromolecular freedom. However, X_c is higher in the composites relative to pure PLA. The maximum change in X_c is observed at 10 wt% e-Lignin loadings, in which the X_c of PLA increased from 8.89% to 35.89%. The excellent dispersion improves the interfacial interaction between the PLA and the e-Lignin chain, resulting in a larger number of nucleating sites, which leads to a high degree of crystallinity [25].

Additionally, the presence of e-Lignin increases the thermal stability of the PLA/e-Lignin composite compared to pure PLA. The T_5 and T_{max} of the composites with different e-Lignin loading fractions are higher than those pure PLA shown in Table 3. This increased degradation temperature results from the abundant aromatic phenyl groups in the e-Lignin. The aromatic structures are very stable owing to the large π bonds formed by the unhybridized p orbitals, which only decompose at very high temperatures. Notably, the degradation of the composites is happed from ~350–400 °C at a faster rate (Figs. 5 b,c), and it is a prerequisite for 3D printing that all composites exhibit excellent thermal stability around 200 °C.

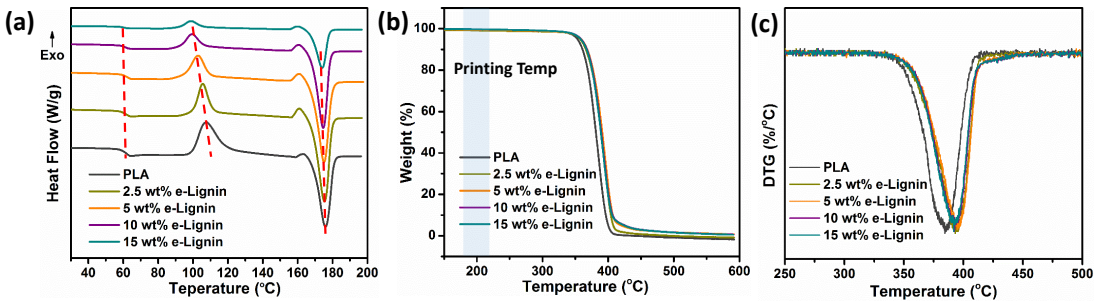

Fig. 5. (a) DSC, (b,c) TGA curves of PLA and PLA/e-Lignin composites.

Table 3. Thermal properties of PLA and PLA/e-Lignin composites

	T_g (°C)	T_{cc} (°C)	T_m (°C)	ΔH_{cc} (J/g)	ΔH_m (J/g)	X_c (%)	T_5 (°C)	T_{max} (°C)
PLA	62.24	108.75	175.93	31.50	39.77	8.89	352.93	384.41
2.5 wt% e-Lignin	62.11	105.80	175.33	22.13	48.35	29.67	357.12	393.26
5 wt% e-Lignin	61.82	103.10	175.20	19.11	47.25	33.62	359.12	395.08
10 wt% e-Lignin	61.11	99.60	174.62	11.16	39.97	35.89	358.72	392.53
15 wt% e-Lignin	60.51	98.90	173.88	5.71	29.34	31.76	357.93	391.90

T_g, T_{cc}, T_m, and X_c are the glass transition temperature, cold crystallization temperature, melting point, and degree of

crystallinity, respectively. ΔH_{cc} and ΔH_m refer to the enthalpy of cold crystallization and enthalpy of melting, respectively. T_5 and T_{max} are the initial thermal degradation temperatures at which 5 wt% mass loss occurs and the maximum weight loss rate occurs, respectively.

The mechanical properties of the PLA/lignin and PLA/e-Lignin composites are compared in **Fig. 6**. The pure PLA shows the tensile strength of 65.9 MPa, modulus of 2.89 GPa, elongation at break of 3.49%, and toughness of 1.49 MJ/m^3 as shown by the dashed lines in **Figs. 6b,c,e,f**. The tensile strength of the composites is reduced by both lignin and e-Lignin incorporation. However, lignin proves to be effective to increase PLA modulus owing to rigid phenyl groups; e.g., the 2.5 wt% lignin PLA composite achieves the highest modulus (3.20 GPa), higher than that of pure PLA (2.89 GPa). While no significant improvement is observed in the modulus of the PLA/e-Lignin composites. Moreover, significantly lower elongations at break and toughness relative to pure PLA were measured for the PLA/lignin composites, which are directly fractured near the yield point without apparent plastic deformation (**Figs. 6a**), exhibiting a typical brittle fracture characteristic. In sharp contrast, obvious ductile fracture behaviors are shown in the PLA/e-Lignin composites (**Fig. 6d**). Particularly, the 10 wt% e-Lignin composite displays an extremely large necking region with an elongation of 25.34% and a toughness of 7.34 MJ/m^3, approximately five times and over seven times compared to that observed with pure PLA, respectively. This result can be explained by the high mobility of the PLA molecular chains after introducing the e-Lignin, which is consistent with the DSC results.

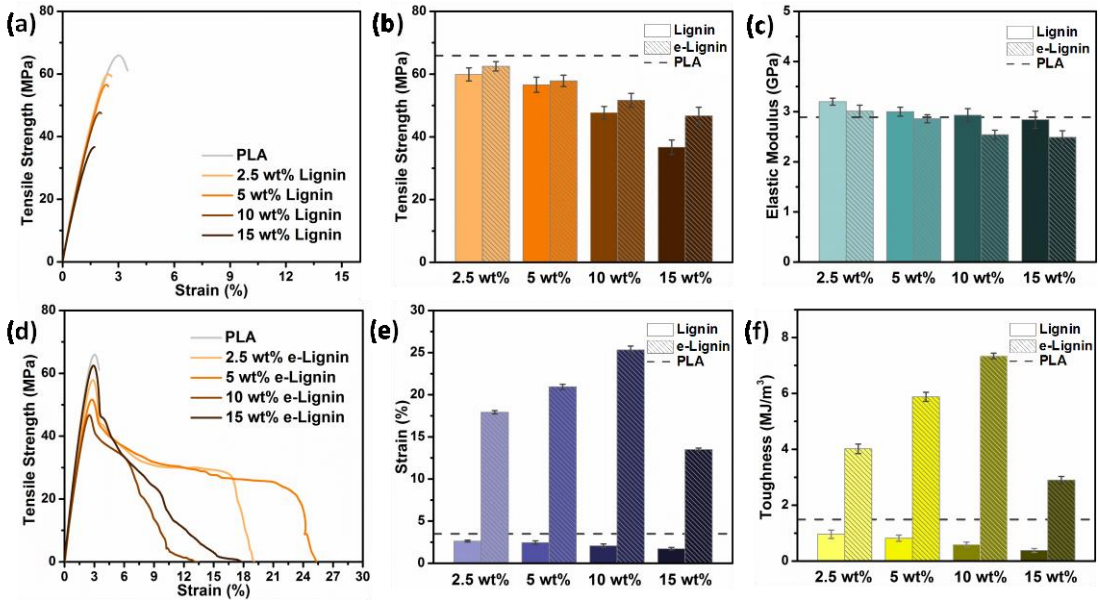

Fig. 6. Stress-strain curves of (a) PLA/lignin composites and (d) PLA/e-Lignin composites made by injection molding. (b) tensile strength, (c) modulus, (e) strain, (f) toughness comparison of PLA/lignin composites and PLA/e-Lignin composites.

4.4 Rheological and thermo-mechanical properties of 3D printed specimens

The 2.5 and 10 wt% e-Lignin composites were selected for 3D printing, and the following analysis was performed. Storage modulus (E') and tan δ curves obtained as a function of temperature for different specimens are shown in Fig. 7a. It can be seen that the E' curves of all the composites are identical in shape, showing a flat plot until 50 °C and then dramatically decreasing at ~60 °C due to glass transition behavior. The E' of pure PLA in the initial stage is 2.54 GPa, which decreases to 1.99 GPa for the 10 wt% e-Lignin composites due to the introduction of e-Lignin with a much lower modulus. However, compared with pure PLA, the tan δ of the 10 wt% e-Lignin composites increases from 2.84 to 3.32 with an increase of 16.9 %. Meanwhile, the T_g gradually decreases from 68.24 to 66.66 °C, similar to the DSC results. These results demonstrate that uniformly dispersed e-Lignin effectively improves the damping properties of the composites, and the thermal mobility of the molecular chains is not restricted [26].

The melt viscosity of the PLA/e-Lignin composites at 210 °C as a function of shear rate is shown in Fig. 7b. All the specimens exhibit shear shining behavior, showing decreased shear viscosity with increasing shear rate, because of the disentanglement during flow at a higher shear rate, ensuring processability in 3D printing. However, compared with pure PLA, the addition of e-lignin decreases the viscosity at a low shear rate. This viscosity is related to the molecular weight of the polymer according to the Mark-Houwink equation [27], in which $[\eta] = KM_w^a$, where K and a are constant. Therefore, the lower viscosity of the PLA/e-Lignin composite is attributed to the smaller molecular weight of the composite resulting from the incorporation of e-Lignin, which has a lower molecular weight relative to PLA shown in Table 4. Notably, there is no significant viscosity difference between the pure PLA and the PLA/e-Lignin composites at a high shear rate. Nguyen et al. reported a melt viscosity and shear rate window for good 3D printability, suggesting a shear rate and viscosity of *ca.* 190 to 3000 s^{-1} and *ca.* 70 to 500 Pa.s, respectively [28]. The flow curves of the investigated specimens show a good fit with the above conditions (Fig. 7b). The digital images shown in Fig. 7c are printed using 2.5 and 10 wt% e-Lignin filaments to visually demonstrate the 3D printability of these samples. Overall, the PLA/e-Lignin composites exhibit excellent printability.

The mechanical properties of the 3D printed specimens are listed in Table 4. As demonstrated, the changing trend in the mechanical properties is similar to that of injection molding. The attractive effects of the addition of e-Lignin on the mechanical properties are the increment toughness (lost energy determined from the area under the stress-strain curve up to break) and impact energy. The maximum toughening effect of the 10 wt% e-Lignin composites corresponded with the highest amount of absorbed energy in the impact test (6.36 KJ/m^2), three times higher than that of pure PLA.

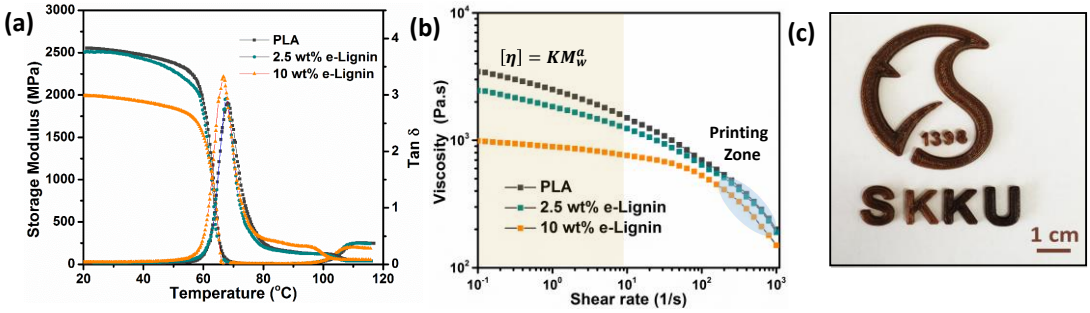

Fig. 7. (a) Storage modulus and damping parameter curves of 3D printed composites. (b) The viscosity of 3D printed composites at 210 °C. (c) Examples of 3D printed objects are made from 10 wt% e-Lignin composites ("K" and "U"), and 2.5 wt% e-Lignin composites (other parts).

Table 4. Mechanical properties of 3D printed specimens

	Modulus (GPa)	Tensile strength (MPa)	Elongation (%)	Toughness (MJ/m^3)	Impact energy (KJ/m^2)
PLA	2.91 ± 0.05	60.8 ± 1.7	2.98 ± 0.10	1.16 ± 1.1	2.12 ± 0.3
2.5 wt% e-Lignin	2.93 ± 0.07	55.2 ± 1.5	7.11 ± 1.31	2.65 ± 1.3	3.04 ± 0.9
10 wt% e-Lignin	2.42 ± 0.03	46.7 ± 1.0	21.7 ± 0.94	3.84 ± 1.3	6.36 ± 1.2

4.5 Toughening mechanism analysis

The cross-section of 3D printed specimens after the impact test is shown in Fig. 8. Different from other manufacturing methods, the fracture of the 3D printed specimens are divided into two types of fractures: the fracture of the filament itself, referred to as "Intra-Filament fracture," and the fracture between different filaments, referred to as "Inter-Filament fracture," as shown in Fig. 8a. The intra-filament fracture of the pure PLA specimens has smooth and laminated fractured surfaces. However, the fracture surface becomes rougher and more irregular with increasing filling content. Particularly, a lot of the e-Lignin particles are pulled out from the matrix of the 10 wt% e-Lignin composites (Fig. 8b). Here, the PLA matrix shows obviously ductile fracture characteristics. Inter-filament fracture is related to adhesion between different layers during printing. Thus, the tear test was employed to study the interlayer adhesion of the 3D printed specimens shown in Fig. 8c. The W is the weld width between two consecutive stacking layers. The weld energy (E) can be calculated as a function of the tear force (F), which is given by E = 2F/W [29]. For the 10 wt% e-Lignin composites, the biggest weld width is observed, showing the best interlayer diffusion caused by the higher mobility of PLA molecular chains. Wherein, it also shows better tear energy of 24.09 N/mm, more than twice that of pure PLA (10.11 N/mm). The improvement in tear energy can be analyzed by the tear fracture morphology shown in Fig. 8d. A clear porous structure is observed due to the removal of the e-Lignin by the applied tear force, indicating that e-Lignin bridges the printed layers and enhances the weld area. Additionally, the surrounding PLA displays obvious ductile deformation.

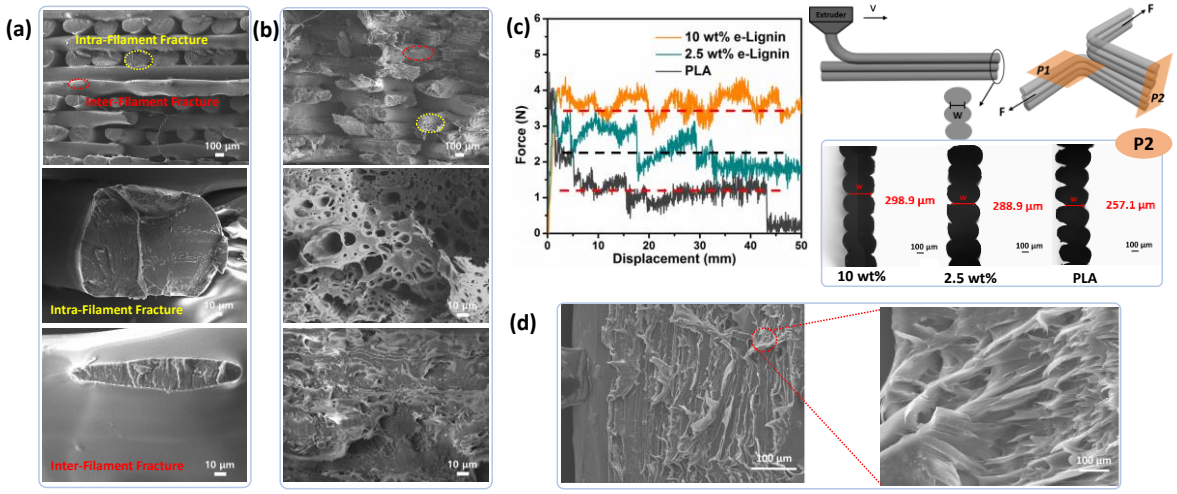

Fig. 8. The cross-section SEM images of (a) pure PLA, (b) 10 wt% e-Lignin composite after impact test, (c) left is tear force-displacement curve, right are schematic diagram and testing configuration of 3D printed single layers specimen, where the tear surface and the cross-section of different layers are P1 and P2 respectively. (d) the P1 plane SEM images of 10 wt% e-Lignin composite after tear test.

Herein, two mechanisms are utilized to explain the toughening effect of 3D printed specimens shown in **Fig. 9**. One is the filler bridging mechanism, in which the ductile e-Lignin particles bridge the different layers and suppress crack growth at the same time, they plastically deform absorbing an additional amount of fracture energy. The other mechanism is the matrix plasticization mechanism. Here, the e-Lignin interacts into the PLA molecular chains through dipole attraction between the ester group of the PLA and e-Lignin. The e-Lignin macromolecule can separate the PLA molecular chains and increase the distance between them, weakening the attractive force within the PLA molecular chains. Therefore, the mobility of the PLA molecular chains is increased when an external load is applied, manifesting as a toughening effect finally.

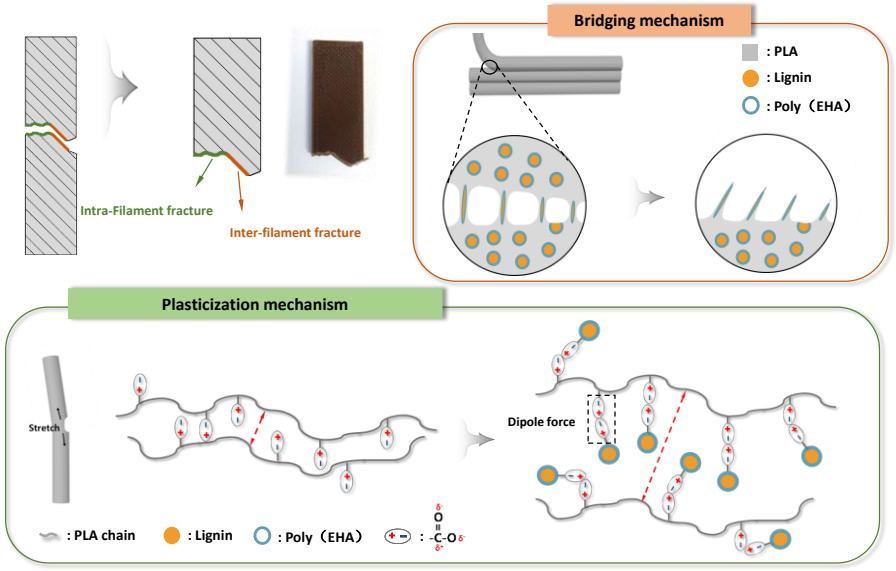

Fig. 9. Toughening diagram of 3D printed PLA/ e-Lignin composites.

5.0 CONCLUSIONS

Lignin, a waste byproduct of the pulp and paper industry was blended with PLA to make high toughness biocomposites compatible with 3D printing through interfacial engineering. The e-Lignin was synthesized by chemically copolymerizing ethylhexyl acrylate monomer onto lignin. Graft modification enabled the e-Lignin to improve its interfacial compatibility with PLA significantly as both have the same ester functional group. The presence of e-Lignin contributed considerably to the increase of toughness. Particularly, the toughness and impact energy of the 10 wt% e-Lignin composites indicated an approximately three-time increase, compared to that of pure PLA. The presence of well-dispersed e-Lignin particles within the PLA induced local relaxation of the polymer chain, which not only shows a plasticization effect on the composites but also promotes the rheological responses that facilitated 3D printing. Notable that better melt diffusion and interfusion between the printed layers were achieved, resulting in high weld energy. More than twice the weld energy was achieved in the 10 wt% e-lignin composites compared with pure PLA. Additionally, some e-Lignin particles also played a bridging role between printed layers. Therefore, ductile lignin-based biocomposites were fabricated by 3D printing, and lignin was converted from a waste stream to a valuable feedstock for additive manufacturing, opening a new route to reducing the present environmental concerns while delivering products with superior mechanical performance.

6.0 DELIVERABLES

- Conference Publications

"Ductile PLA/Lignin biocomposite for 3D printing" *The Korean Society for Composite Materials,* Fall Conference (2020)
"Reinforcement of polylactic acid (PLA) bio-composite with lignin from oil palm empty fruit bunches (OPEFB) for 3D printing application" *International Conference Biotechnology Engineering* 2021 (ICBioE 21)
"Poly(lactic) acid reinforced with alkaline lignin biocomposites prepared by thermal extrusion for sustainable 3D printing process" *International conference on material processing and technology* 2021

- Journal Publications

"Ductile PLA/lignin-g-poly (2-Ethylhexyl acrylate) biocomposite for fused deposition modeling." *Composite Part B: engineering*. Ready for submission
"Review on solvent extraction methods of lignin from oil palm empty fruit bunches (OPEFB). " *Journal of Natural Fibers*. Under review
"Fabrication of sustainable poly(lactic) acid reinforced alkaline lignin biocomposite extracted from oil palm empty fruit bunch (OPEFB)." *Industrial Crop and Products*. Under review
"Mechanical and thermal properties of polylactic acid filled lignin powder biocomposite filaments with epoxidized palm oil for sustainable 3D printing application." *PERINTIS eJournal* 11.1 (2021): 23-39.
"Extraction of lignin from oil palm empty fruit bunches (OPEFB) as filler in polylactic acid (PLA) biocomposite for 3D printing application" *Journal of Engineering Science and Technology*. Submission.

7.0 REFERENCES

[1] Tabone MD, Cregg JJ, Beckman EJ, Landis AE. Sustainability metrics: life cycle assessment and green design in polymers. Environmental science & technology. 2010;44(21):8264-9.

[2] Ramesh P, Vinodh S. State of art review on Life Cycle Assessment of polymers. International Journal of Sustainable Engineering. 2020;13(6):411-22.

[3] Harding K, Dennis J, Von Blottnitz H, Harrison S. Environmental analysis of plastic production processes: Comparing petroleum-based polypropylene and polyethylene with biologically-based poly-β-hydroxybutyric acid using life cycle analysis. Journal of biotechnology. 2007;130(1):57-66.

[4] Tekinalp HL, Meng X, Lu Y, Kunc V, Love LJ, Peter WH, et al. High modulus biocomposites via additive manufacturing: Cellulose nanofibril networks as "microsponges". Composites Part B: Engineering. 2019;173:106817.

[5] Vaidya AA, Collet C, Gaugler M, Lloyd-Jones G. Integrating softwood biorefinery lignin into polyhydroxybutyrate composites and application in 3D printing. Materials Today Communications. 2019;19:286-96.

[6] Domínguez-Robles J, Martin NK, Fong ML, Stewart SA, Irwin NJ, Rial-Hermida MI, et al. Antioxidant PLA composites containing lignin for 3D printing applications: A potential material for healthcare applications. Pharmaceutics. 2019;11(4):165.

[7] Kuo C-C, Liu L-C, Teng W-F, Chang H-Y, Chien F-M, Liao S-J, et al. Preparation of starch/acrylonitrile-butadiene-styrene copolymers (ABS) biomass alloys and their feasible evaluation for 3D printing applications. Composites Part B: Engineering. 2016;86:36-9.

[8] Tarrés Q, Melbø JK, Delgado-Aguilar M, Espinach F, Mutjé P, Chinga-Carrasco G. Bio-polyethylene reinforced with thermomechanical pulp fibers: Mechanical and micromechanical characterization and its application in 3D-printing by fused deposition modelling. Composites Part B: Engineering. 2018;153:70-7.

[9] Voet VS, Strating T, Schnelting GH, Dijkstra P, Tietema M, Xu J, et al. Biobased acrylate photocurable resin formulation for stereolithography 3D printing. Acs Omega. 2018;3(2):1403-8.

[10] Maturi M, Pulignani C, Locatelli E, Buratti VV, Tortorella S, Sambri L, et al. Phosphorescent bio-based resin for digital light processing (DLP) 3D-printing. Green Chemistry. 2020;22(18):6212-24.

[11] Gleuwitz FR, Sivasankarapillai G, Siqueira G, Friedrich C, Laborie M-PG. Lignin in bio-based liquid crystalline network material with potential for direct ink writing. ACS Applied Bio Materials. 2020;3(9):6049-58.

[12] Thibaut C, Denneulin A, Du Roscoat SR, Beneventi D, Orgéas L, Chaussy D. A fibrous cellulose paste formulation to manufacture structural parts using 3D printing by extrusion. Carbohydrate polymers. 2019;212:119-28.

[13] Napper IE, Thompson RC. Environmental deterioration of biodegradable, oxo-biodegradable, compostable, and conventional plastic carrier bags in the sea, soil, and open-air over a 3-year period. Environmental science & technology. 2019;53(9):4775-83.

[14] Liu J, Sun L, Xu W, Wang Q, Yu S, Sun J. Current advances and future perspectives of 3D printing natural-derived biopolymers. Carbohydrate polymers. 2019;207:297-316.

[15] Gkartzou E, Koumoulos EP, Charitidis CA. Production and 3D printing processing of bio-based thermoplastic filament. Manufacturing Review. 2017;4:1.

[16] Wasti S, Triggs E, Farag R, Auad M, Adhikari S, Bajwa D, et al. Influence of plasticizers on thermal and mechanical properties of biocomposite filaments made from lignin and polylactic acid for 3D printing. Composites Part B: Engineering. 2021;205:108483.

[17] Nguyen NA, Bowland CC, Naskar AK. A general method to improve 3D-printability and inter-layer adhesion in lignin-based composites. Applied Materials Today. 2018;12:138-52.

[18] Obielodan J, Vergenz K, Aqil D, Wu J, Mc Ellistrem L. Characterization of PLA/Lignin Biocomposites for 3D Printing.

[19] Tanase-Opedal M, Espinosa E, Rodríguez A, Chinga-Carrasco G. Lignin: A biopolymer from forestry biomass for biocomposites and 3D printing. Materials. 2019;12(18):3006.

[20] Mimini V, Sykacek E, Syed Hashim SNA, Holzweber J, Hettegger H, Fackler K, et al. Compatibility of kraft lignin, organosolv lignin and lignosulfonate with PLA in 3D printing. Journal of Wood Chemistry and Technology. 2019;39(1):14-30.

[21] Kim Y, Suhr J, Seo H-W, Sun H, Kim S, Park I-K, et al. All biomass and UV protective composite composed of compatibilized lignin and poly (lactic-acid). Scientific Reports. 2017;7(1):1-11.

[22] Lyu Y, Chen Y, Lin Z, Zhang J, Shi X. Manipulating phase structure of biodegradable PLA/PBAT system: Effects on dynamic rheological responses and 3D printing. Composites Science and Technology. 2020;200:108399.

[23] Davis CS, Hillgartner KE, Han SH, Seppala JE. Mechanical strength of welding zones produced by polymer extrusion additive manufacturing. Additive manufacturing. 2017;16:162-6.

[24] Sun Y, Ma Z, Xu X, Liu X, Liu L, Huang G, et al. Grafting lignin with bioderived polyacrylates for low-cost, ductile, and fully biobased poly (lactic acid) composites. ACS Sustainable Chemistry & Engineering. 2020;8(5):2267-76.

[25] Llanes LC, Clasen SH, Pires AT, Gross IP. Mechanical and thermal properties of poly (lactic acid) plasticized with dibutyl maleate and fumarate isomers: Promising alternatives as biodegradable plasticizers. European Polymer Journal. 2021;142:110112.

[26] Wei W, Zhang Y, Liu M, Zhang Y, Yin Y, Gutowski WS, et al. Improving the damping properties of nanocomposites by monodispersed hybrid POSS nanoparticles: Preparation and mechanisms. Polymers. 2019;11(4):647.

[27] Chuah H, Lin-Vien D, Soni U. Poly (trimethylene terephthalate) molecular weight and Mark–Houwink equation. Polymer. 2001;42(16):7137-9.

[28] Nguyen NA, Barnes SH, Bowland CC, Meek KM, Littrell KC, Keum JK, et al. A path for lignin valorization via additive manufacturing of high-performance sustainable composites with enhanced 3D printability. Science advances. 2018;4(12):eaat4967.

[29] Seppala JE, Han SH, Hillgartner KE, Davis CS, Migler KB. Weld formation during material extrusion additive manufacturing. Soft Matter. 2017;13(38):6761-9.